Clustered ventilation defects and bilinear respiratory reactance in asthma

Graham M. Donovan

Department of Mathematics, University of Auckland, Private Bag 92019, Auckland, New Zealand

HIGHLIGHTS

- Clustered ventilation defects are a hallmark of asthma observed in imaging studies.
- We present a new model of clustered ventilation defect formation in the lung.
- Noise-driven defect formation in asymmetric trees yields a combination of structural and dynamic defect formation.
- The reactance versus flow curve is bilinear, but the breakpoint is not coincident with the clustering bifurcation.

ARTICLE INFO

ABSTRACT

Imaging studies of asthmatics typically reveal clustered ventilation patterns, rather than homogeneous ventilation; furthermore, the variation of these clusters suggests that the causes are at least partially dynamic, rather than structural. Theoretical studies have indicated dynamic mechanisms by which homogeneous ventilation solutions lose stability and clustered solutions emerge. At the same time, it has been demonstrated experimentally that respiratory reactance characteristically has a bilinear relationship with lung volume, and that changes to this relationship are indicative of various aspects of disease progression and control. Moreover, the transition point in the bilinear reactance relationship is thought to relate to reopening/recruitment of airway units, and thus may be connected to the bifurcation via which clustered ventilation solutions emerge. In order to investigate this possibility we develop a new model, including both airway–airway coupling and airway–parenchymal coupling, which exhibits both clustered ventilation defects and also a bilinear reactance relationship. Studying this model reveals that (1) the reactance breakpoint is not coincident with the bifurcation; (2) numerous changes to underlying behaviour can alter the reactance breakpoint in ways which mimic the experimental data; and (3) the location of ventilation defects can be a combination of both structural and dynamic factors.

1. Introduction

Clustered ventilation defects are a hallmark of asthma, wherein reversible airway narrowing occurs in a spatially organised way such that both hypo- and hyper-ventilated regions emerge (e.g. Tzeng et al., 2009; Layachi et al., 2013; Simon et al., 2012). Because these regions can vary from event to event, the causes are thought to be at least partially dynamic (Venegas et al., 2005; Leary et al., 2014), as opposed to structural, and understanding how and why they occur may shed light on the basic pathophysiology of asthma, which is not well understood.

Several theoretical models have been developed which address the formation of clustered ventilation defects (VDefs). Best known is the computational work of Venegas, Winkler and colleagues,

based on Anafi and Wilson (2001) and extended to a symmetric airway tree, beginning with Venegas et al. (2005) and used in numerous subsequent studies (e.g. Winkler and Venegas, 2007; Golnabi et al., 2014; Wongviriyawong et al., 2010; Winkler et al., 2015; Leary et al., 2014). The model of Donovan and Kritter (2015) employs similar ideas, but is constructed in such a way as to allow some degree of analytic understanding of how and why clustered VDefs occur (for example, analytic eigenvalues and eigenvectors allow understanding of the unstable modes of the system). However Donovan and Kritter (2015) made a significant assumption in neglecting the role of the conducting airway tree (airway–airway coupling), instead of relying on interactions among physically adjacent respiratory bronchioles and their dependent tissue (airway–parenchymal coupling) to drive clustered VDef formation. This approach has two key drawbacks: (1) the neglected role of the conducting airway tree is unclear and (2) without the upstream

E-mail address: g.donovan@auckland.ac.nz

airways, it is difficult or impossible to incorporate models of measured lung function.

Here we are driven to investigate the experimental results of Kelly et al. (2012, 2013), which demonstrate the utility of measuring respiratory reactance as a function of lung volume. These authors show that this relationship is reliably bilinear, and that the handful of parameters associated with that bilinear form are useful markers of lung function, asthma severity and asthma control. Furthermore, they postulate that the "breakpoint" in their bilinear form is related to reopening/recruitment of airway units. Such a transition, then, might be related to the bifurcation which occurs between homogeneous and clustered ventilation in the models of Donovan and Kritter (2015) and Venegas et al. (2005). The hypothesis is made more plausible by other evidence of the relationship between ventilation heterogeneity and impedance, e.g. Kaczka et al. (2009, 2011) and Lutchen et al. (2001). Thus, one interesting question is if the breakpoint and bifurcation are coincident.

In order to answer this question, we first construct a new model, based on Donovan and Kritter (2015), but now incorporating airway–airway coupling via flow through the conducting airway tree. This is necessary, in the first instance, because existing reactance (impedance) models require the behaviour of the conducting tree, but it also has the significant advantage that we are able to assess other theoretical implications of the previously neglected components.

This paper is then structured as follows. First, we augment the model of Donovan and Kritter (2015) to incorporate a conducting airway tree (with arbitrary geometry); this is not conceptually difficult, but leads to challenges associated with the resulting system of differential-algebraic equations (DAEs). Rather than attempting to solve the DAEs directly, we instead present a procedure which allows elimination of the algebraic constraints in any tree, resulting in a system of ordinary differential equations only. This eases both computational and theoretical issues considerably.

Using this newly developed model, then, we are able to show: (1) the bifurcation between homogeneous and clustered ventilation seen in Donovan and Kritter (2015) persists with the inclusion of airway–airway coupling via flow through the conducting airways; (2) the characteristic bilinear reactance relationship also that occurs in this model, but (3) the breakpoint and bifurcation that are *not* coincident. Instead the reactance breakpoint appears to reflect a transition driven by the highly nonlinear relationship between radius and impedance (and, because of the dependence between flow and radius, between flow and impedance). We also examine the locations and persistence of the locations of ventilation defects; that is, the extent to which they are dynamic as opposed to structural.

We further consider the ways in which the bilinear reactance parameters can be altered by the underlying system, suggesting ways in which asthmatic pathophysiology may differ from non-asthmatics; however, there are many potential combinations which lead to the same sort of changes in that relationship, and hence the inversion from observed data to underlying behaviour is not unique.

2. Model

Here we develop a new model based on Donovan and Kritter (2015) (which considers only the respiratory bronchioles), but now with the inclusion of an arbitrary conducting tree. Many of the underlying ideas are shared with Venegas and Winkler et al. (Venegas et al., 2005; Winkler and Venegas, 2007; Golnabi et al., 2014; Wongviriyawong et al., 2010; Winkler et al., 2015), and there are structural similarities with Stewart and Jensen (2015).
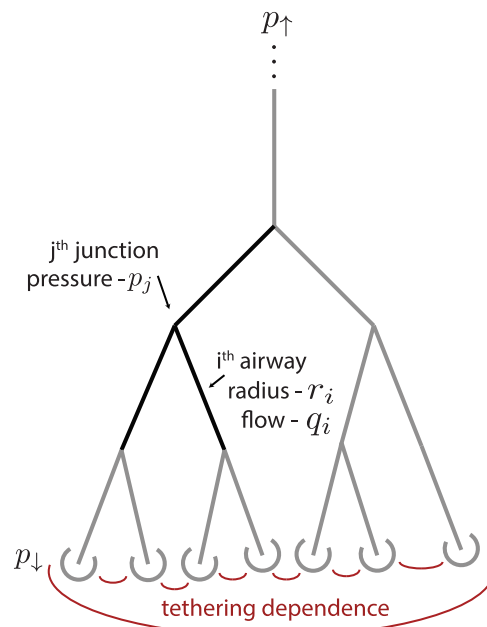
Fig. 1. Schematic illustration of model geometry and symbols. Two types of coupling are considered: airway–airway coupling via flow through the conducting airways (black and grey), and coupling via parenchymal interdependence (red). (For interpretation of the references to colour in this figure caption, the reader is referred to the web version of this paper.)

The setup is simple: we have airway luminal radius (r_i) and flow (q_i) in each airway, and pressure p_j at each junction[1]; these can be arranged in an arbitrary branching tree with $i = 1\ldots N$ airways and $j = 1\ldots M$ junctions. We denote the boundary pressures at the "top" of the tree $p_\uparrow$ (e.g. at the trachea in a full tree), and driving pressure $p_\downarrow$ and the "bottom" of the respiratory bronchioles. The arrangement is illustrated schematically in Fig. 1.

The evolution of these radii, pressures and flows is then given by: (1) the airway dynamics (including narrowing driven by ASM); (2) conservation of flow at the junctions; and (3) flow equations along each airway. That is, for each airway we have dynamics given by

$$\dot{r}_i = \rho\big(\boldsymbol{\phi}(r_i; \boldsymbol{r}, \boldsymbol{p}, \boldsymbol{q}) - r_i\big) \tag{1}$$

based on Donovan and Kritter (2015) where $\boldsymbol{\phi}$ is based on quasi-static experimental measurements and the construction gives first-order kinetics about those equilibria with timescale ρ. (Full details of $\boldsymbol{\phi}$ are presented in Section 2.2, but for now are neglected for clarity.)

At each junction, we have conservation of flow

$$q_m = q_{d_1} + q_{d_2} \tag{2}$$

where the notation here indicates the mother and two daughter branches at each junction. We will later re-write this in terms of connectivity matrices.

Then in each airway, we assume Poiseuille flow

$$\Delta p_i = \alpha_i r_i^{-4} q_i \tag{3}$$

where Δp_i is the pressure difference from top to bottom of the ith airway (again, later in terms of connectivity matrices) and for compactness of notation we have combined the parameters associated with the flow into a single constant α_i for each airway.[2]

---

[1] Here we neglect the pressure loss factor of Lambert et al. (1982).
[2] We present the model development in dimensional terms; units are parameter values are given in Appendix A.

To complete this set of equations, we consider two types of boundary conditions:

1. *Pressure-controlled* boundary conditions prescribe both $p_\uparrow$ and $p_\downarrow$. Narrowing airways by stimulating ASM will result in reduced flow.
2. *Flow-controlled* boundary conditions prescribe $p_\uparrow$ and $q_\uparrow = \hat{q}$, allowing $p_\downarrow$ to vary in order to maintain this flow despite airway narrowing.

While true breathing control is certainly more complicated, these two cases can be though of as the extremes of idealised control.

By way of comparison with previous work, Donovan and Kritter (2015) considered tethering dependence (Eq. (1)) but only in the terminal airways, which were assumed to be fed homogeneously by a bulk representation of the conducting airways. In that case, both Eqs. (2) and (3) are replaced with boundary conditions, and so the resulting system consists of ODEs only. Incorporating the conducting tree explicitly yields instead a set of differential-algebraic equations. While in principle it is possible to solve these directly, in this case they can be simplified to ODEs, which greatly eases both numerical and theoretical issues.

2.1. Eliminating the algebraic constraints

First we re-write the governing equations in terms of connectivity matrices for a general tree. We have $j = 1 \ldots M$ junctions, $i = 1 \ldots N$ airways, so $\boldsymbol{p} = [p_1 \ldots p_M]^\top$, $\boldsymbol{r} = [r_1 \ldots r_N]^\top$, $\boldsymbol{q} = [q_1 \ldots q_N]^\top$. (In this section we use the notation convention that scalars are denoted by lower case; vectors by lower case in bold type; and matrices by capitals in bold type.).

Then the connectivity matrices $\mathbf{C}_{J^+}, \mathbf{C}_{J^-}$ relate airways to junctions (and are size $N \times M$), and $\mathbf{C}_{I^+}, \mathbf{C}_{I^-,1}, \mathbf{C}_{I^-,2}$ relate junctions to airways (size $M \times N$) – that is, the radii of the "mother" airways of each junction are given by

$$\mathbf{C}_{I^+}\boldsymbol{r} \tag{4}$$

and of the (arbitrarily numbered) first and second "daughter" airways by $\mathbf{C}_{I^-,1}\boldsymbol{r}$ and $\mathbf{C}_{I^-,2}\boldsymbol{r}$ respectively. Here the plus and minus notation ($\mathbf{M}_{(\cdot)^+}$ and $\mathbf{M}_{(\cdot)^-}$) refers to connectivity matrices which transfer "up" and "down" the tree, respectively (that is, $+$ toward the trachea and $-$ toward the terminal bronchioles).

Incorporating the pressure boundary conditions we define an operator for the pressures at the top and bottom of each airway as

$$\gamma_{J^+}(\boldsymbol{p}) = \mathbf{C}_{J^+}\boldsymbol{p} + p_\uparrow \boldsymbol{v}_\uparrow \tag{5}$$

where $\boldsymbol{v}_\uparrow$ is one for the topmost airway and zero otherwise, and

$$\gamma_{J^-}(\boldsymbol{p}) = \mathbf{C}_{J^-}\boldsymbol{p} + p_\downarrow \boldsymbol{v}_\downarrow \tag{6}$$

with $\boldsymbol{v}_\downarrow$ selecting the terminal (order 1)[3] airways. Here the down arrow notation $(\cdot)_\downarrow$ indicates quantities associated with the "bottom" (terminal) boundary of the tree, while the up arrow notation $(\cdot)_\uparrow$ is associated with the upper boundary (see Fig. 1).

Then $\Delta\boldsymbol{p}$ (length N, associated with each airway) is given by

$$\Delta\boldsymbol{p} = \gamma_{J^+}(\boldsymbol{p}) - \gamma_{J^-}(\boldsymbol{p}). \tag{7}$$

Thus in vector form the Poiseuille equations become

$$\boldsymbol{q} = \boldsymbol{\alpha}^{\circ(-1)} \circ \boldsymbol{r}^{\circ 4} \circ \Delta\boldsymbol{p} \tag{8}$$

$$= \boldsymbol{\alpha}^{\circ(-1)} \circ \boldsymbol{r}^{\circ 4} \circ \left[(\mathbf{C}_{J^+} - \mathbf{C}_{J^-})\boldsymbol{p} + p_\uparrow \boldsymbol{v}_\uparrow - p_\downarrow \boldsymbol{v}_\downarrow \right] \tag{9}$$

where the notation $\circ$ indicates the element-by-element Hadamard vector product,[4] and similarly in the exponents (e.g. $\boldsymbol{\alpha}^{\circ(-1)} = \left[(\alpha_1)^{-1}, (\alpha_2)^{-1}, \ldots, (\alpha_N)^{-1} \right]^\top$). In the same way the flow conservation equations become

$$(\mathbf{C}_{I^+} - \mathbf{C}_{I^-,1} - \mathbf{C}_{I^-,2})\left[\boldsymbol{\alpha}^{\circ(-1)} \circ \boldsymbol{r}^{\circ 4} \circ \left\{ (\mathbf{C}_{J^+} - \mathbf{C}_{J^-})\boldsymbol{p} + p_\uparrow \boldsymbol{v}_\uparrow - p_\downarrow \boldsymbol{v}_\downarrow \right\} \right]$$
$$= 0. \tag{10}$$

Noting that this is linear in $\boldsymbol{p}$, we solve to obtain

$$\boldsymbol{p} = \mathbf{W}^{-1}(\mathbf{C}_{I^+} - \mathbf{C}_{I^-,1} - \mathbf{C}_{I^-,2})\left[\boldsymbol{\alpha}^{\circ(-1)} \circ \boldsymbol{r}^{\circ 4} \circ \left\{ p_\uparrow \boldsymbol{v}_\uparrow - p_\downarrow \boldsymbol{v}_\downarrow \right\} \right] \tag{11}$$

where

$$\mathbf{W} = (\mathbf{C}_{I^+} - \mathbf{C}_{I^-,1} - \mathbf{C}_{I^-,2})\mathbf{D}_{\boldsymbol{\alpha}^{\circ(-1)} \circ \boldsymbol{r}^{\circ 4}}(\mathbf{C}_{J^+} - \mathbf{C}_{J^-}) \tag{12}$$

and $\mathbf{D}_{\boldsymbol{\alpha}^{\circ(-1)} \circ \boldsymbol{r}^{\circ 4}}$ is the diagonal matrix with the vector $\boldsymbol{\alpha}^{\circ(-1)} \circ \boldsymbol{r}^{\circ 4}$ along the diagonal.

Thus we have found $\boldsymbol{q}$ in terms of $\boldsymbol{r}$ and $\boldsymbol{p}$, and $\boldsymbol{p}$ in terms of $\boldsymbol{r}$. If pressure control is employed, these equations are sufficient – we need to only substitute Eqs. (9) and (11) into (1) to obtain our system of ODEs. However, if we instead have flow control, then simultaneously we have that the sum of the flows in the terminal airways[5] must be equal to $\hat{q}$ and so we can solve to obtain

$$p_\downarrow = \frac{\left\{ \sum_{k \in O(1)} \frac{r_k^4}{\alpha_k} \left[\mathbf{C}_{J^+}\boldsymbol{p} \right]_k \right\} - \hat{q}}{\sum_{k \in O(1)} r_k^4 / \alpha_k} \tag{13}$$

where the notation $k \in O(1)$ indicates order 1 airways. Equivalently, noting that $\sum_{k \in O(1)} \beta_k = \boldsymbol{\beta} \cdot \boldsymbol{v}_\downarrow$, we can write this in vector form as

$$p_\downarrow = \frac{(\boldsymbol{\alpha}^{\circ(-1)} \circ \boldsymbol{r}^{\circ 4} \circ \mathbf{C}_{J^+}\boldsymbol{p}) \cdot \boldsymbol{v}_\downarrow - \hat{q}}{(\boldsymbol{\alpha}^{\circ(-1)} \circ \boldsymbol{r}^{\circ 4}) \cdot \boldsymbol{v}_\downarrow}. \tag{14}$$

Substituting and solving yield

$$\boldsymbol{p} = \Lambda^{-1}\mathbf{W}^{-1}\mathbf{C}_I \mathbf{D}_{\boldsymbol{\alpha}^{\circ(-1)} \circ \boldsymbol{r}^{\circ 4}}\left(-p_\uparrow \boldsymbol{v}_\uparrow - \frac{1}{\lambda}\hat{q}\boldsymbol{v}_\downarrow \right) \tag{15}$$

where $\lambda = (\boldsymbol{\alpha}^{\circ(-1)} \circ \boldsymbol{r}^{\circ 4}) \cdot \boldsymbol{v}_\downarrow$ and

$$\Lambda = \mathbf{I} - \frac{1}{\lambda}\mathbf{W}^{-1}\mathbf{C}_I \mathbf{D}_{\boldsymbol{\alpha}^{\circ(-1)} \circ \boldsymbol{r}^{\circ 4}}\left(\boldsymbol{v}_\downarrow \otimes \boldsymbol{v}_\downarrow \right)\mathbf{D}_{\boldsymbol{\alpha}^{\circ(-1)} \circ \boldsymbol{r}^{\circ 4}}\mathbf{C}_{J^+}. \tag{16}$$

Here $\mathbf{C}_I = \mathbf{C}_{I^+} - \mathbf{C}_{I^-,1} - \mathbf{C}_{I^-,2}$ and $\otimes$ is the vector outer product.

Thus we can eliminate the algebraic constraints in either case and obtain only ODEs. Using

$$\dot{\boldsymbol{r}} = \rho\left(\phi(\boldsymbol{r}, \boldsymbol{q}, \boldsymbol{p}) - \boldsymbol{r} \right) \tag{17}$$

we have $\boldsymbol{q}$ from Eq. (9), and $\boldsymbol{p}$ from either (11) or (15), depending on pressure or flow control, respectively. In either case, the result is a system of ODEs in terms of connectivity matrices for an arbitrary tree.

2.2. Airway dynamics[6]

Here we outline the form of Eq. (1), based on Donovan and Kritter (2015) but modified for the present situation. The

---

[3] We use the Horsfield order scheme to classify airways, with order 1 airways being the smallest airways at the "bottom" of the tree and progressively increasing with larger airways (Horsfield et al., 1971).

[4] Familiar to many as .* in matlab.
[5] It would appear to be simpler to set the top flow equal to $\hat{q}$; this approach is equivalent, due to flow conservation, but is convenient for the calculations that follow.
[6] In this section all quantities are scalars and the scalar/vector/matrix notation used in Section 2.1 is relaxed so as to use common notation with previous work.

underlying idea is that quasi-static experimental data provide the equilibria, about which first order dynamics apply.

For the equilibria we have $\phi = R(P_{tm}(r))$ by composition, where $R(P_{tm})$ describes airway radius as a function of transmural pressure according to

$$R(P_{tm}) = \begin{cases} \sqrt{R_i^2(1 - P_{tm}/P_A)^{-n_A}}, & P_{tm} \leq 0 \\ \sqrt{r_{imax}^2 - (r_{imax}^2 - R_i^2)(1 - P_{tm}/P_B)^{-n_B}}, & P_{tm} > 0 \end{cases} \tag{18}$$

from Lambert et al. (1982) where R_i, r_{imax}, P_A, P_B, n_A and n_B are parameters from that paper, with notation adapted from Politi et al. (2010) (see Appendix A). Here $P(r)$ gives transmural pressure as a function of the radius as

$$P_{tm}(r_i) = p_{mid_i} - \frac{\kappa R_{ref}}{r_i} + \tau(r_i). \tag{19}$$

Note the mid-airway pressure $\boldsymbol{p}_{mid}$ is easily obtained by $\frac{1}{2}\left[\gamma_{J^+}(\boldsymbol{p}) + \gamma_{J^-}(\boldsymbol{p})\right]$. The second term on the right hand side is the constricting pressure of airway smooth muscle (represented by the smooth muscle pressure κ, with $1/r_i$ from the Laplace law for thin-walled cylinders[7] and R_{ref} as a normalising reference radius), and the third is the so-called *parenchymal tethering pressure*. This arises from the restoring forces generated by the parenchymal tissue surrounding the airway, and is described by

$$\tau(r_i) = 2\mu\left(\left(\frac{R_{ref} - r_i}{R_{ref}}\right) + 1.5\left(\frac{R_{ref} - r_i}{R_{ref}}\right)^2\right) \tag{20}$$

according to Lai-Fook (1979), where μ is the parenchymal shear modulus, which crucially *is dependent on lung inflation*. This provides coupling via the parenchymal interdependence (see Fig. 1).

Here for the respiratory bronchioles, as in Donovan and Kritter (2015) we use the local effect that the shear modulus is a function of the local inflation via mean local flow, so that

$$2\mu_i = 0.7 \times \frac{A}{3}\left(|q_i| + |q_{i_l}| + |q_{i_r}|\right) \tag{21}$$

where the parameter A represents the coupling strength and q_{i_l} and q_{i_r} are the respiratory bronchioles to the left and right, respectively.

For the upstream airways, the shear modulus is the average of the shear moduli of the downstream order 1 airways, (that is, the inflation of the parenchyma surrounding an upstream airway is determined by the flow to its dependent tissue) so that

$$\mu_i = \frac{1}{|\mathcal{D}_i|} \sum_{\ell \in \mathcal{D}_i} \mu_\ell \tag{22}$$

where $\mathcal{D}_i$ is the set of order 1 airways downstream from the ith airway. Additional model details, including tree generation, impedance calculation, and parameters are given in Appendix A.

3. Results

We begin by assessing the existence of clustered ventilation defects in the model; while the tethering dependence model of Donovan and Kritter (2015) suggests the presence of such solutions, at least in the flow-controlled case, it is unclear a priori how the inclusion of airway–airway coupling via flow will alter the stability. However, in the flow-controlled case, clustered ventilation solutions are not difficult to find; simply setting the value of

smooth muscle tension κ within the physiological range, and ramping the flow control parameter $\hat{q}$, we see in Fig. 2 the transition between homogeneous and clustered ventilation solutions at steady state. The lower panels give sample distributions within the heterogeneous solutions, at $\hat{q} = 7.9$, 12.8, and 17.7. (Here we give dimensionless values; see Appendix A for dimensional equivalence.) Note that the "homogeneous" solutions (e.g. $\hat{q} > 20$ in Fig. 2(a)) are not truly homogeneous but show variation which reflects the structural variability within the population of open airways. In symmetric trees, on the other hand, solutions are homogeneous (at least across each order/generation in the tree). As in Donovan and Kritter (2015), no clustered ventilation solutions were found when using pressure-control, so we confine ourselves to the flow controlled case from here forward.

Here we have used the asymmetric, $\Delta = 1$ trees of Horsfield et al. (1971). Because these flow paths in these trees are not all equivalent (as in a symmetric tree), the ventilation patterns which emerge have a structural component (as opposed to the purely dynamic patterns of Donovan and Kritter (2015) and Venegas et al. (2005)). In order to demonstrate this more clearly, in Fig. 3 we look at the effect of perturbing the system with random noise of varying standard deviation (additive white noise; see Appendix A). The left hand grid (panel a) shows individual stochastic realisations, with each row having the same noise standard deviation; these are coloured by normalised radius, with black being zero (closed) and red being 1 (open), as in Fig. 2. The right-hand grid (b) quantifies the variation explicitly, giving a measure of the coherent variation[8] for each airway across multiple simulations (100 simulations were used for calculating the variation, not just the 5 shown explicitly.) The rows are common across both panels, each corresponding to the stated noise level; thus by looking "across" any given row, we have individual realisations in panel (a), and the corresponding average variation in panel (b) (that is, airways which are black in panel (b) are always the same in (a), while those which are green in (b) are always changing in (a); note that the variation in (b) is computed from 100 realisations, only five of which are shown explicitly in the corresponding row of panel (a)). We see that varying noise levels allows different balance between structural and dynamic components to clustered ventilation patterns. With too little noise – for example, looking at the top row – the structural patterns persist; the five realisations in panel (a) are visually identical, and indeed the averaged variation in panel (b) shows essentially no variation. Thus here the patterns are determined by structure alone. On the other hand, with too much noise, heterogeneous solutions occur, but clusters break up with random variation between individual airways; see, for example, the bottom row. Now the variation is dominated by noise, with the sample realisations in (a) showing more airway-to-airway variation, and fewer clusters; this is reflected in the measure of variation (panel (b)) by the uniformity across all airways. In between these two extremes of too little and too much noise, there is a small noise region ($\sigma \sim [0.001, 0.01]$),[9] represented by the middle rows, wherein the contributions between structural and dynamic patterns are roughly in balance. Here the realisations show clustered ventilation defects, but with random switching of the VDef pattern, and this is reflected by clustered coherent variation in panel (b). Thus there is an expected trade-off in the noise driven system with structural asymmetry: for small noise, the structural asymmetries dominate the ventilation patterns; for large noise, noise dominates and clustered solutions begin to break down into individual airway variation; in the intermediate regime, with noise and structure approximately in balance, clustered solutions exist

---

[7] Though airway models without this assumption do exist, e.g. Brook et al. (2010).

[8] See Appendix A.

[9] It is worth noting that the precise noise figure is parameter dependent; other parts of parameter space are less noise sensitive.
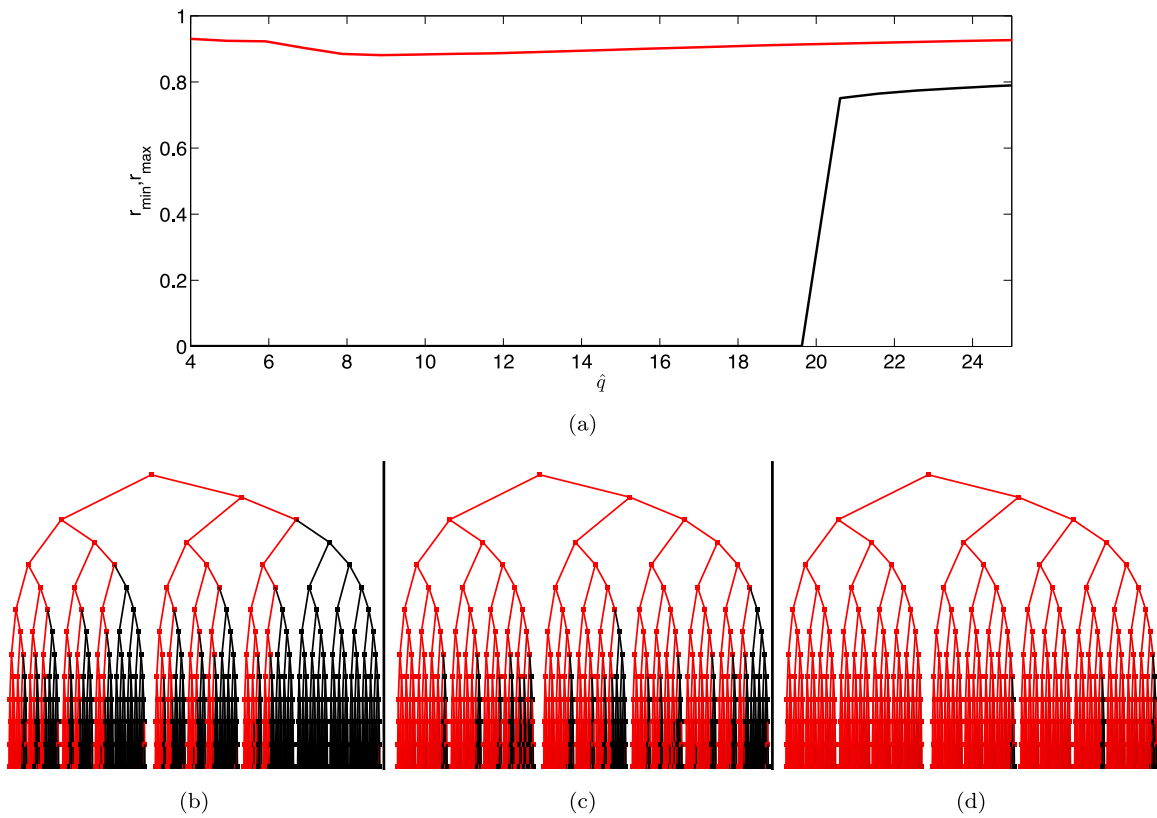
Fig. 2. Heterogeneous and homogeneous ventilation solutions at steady state. Panel (a): maximum and minimum radius of order 1 airways at steady state as $\hat{q}$ is varied; note the transition from heterogeneous solutions to (near) uniform ventilation around $\hat{q} = 20$. Lower panels (b–d): examples of heterogeneous ventilation showing clustering patterns within the tree. Airways are coloured by normalised radius, with black being zero (closed) and red being 1 (open). The panels are at $\hat{q} = 7.9$ (b), 12.8 (c), and 17.7 (d). Here $A = 0.2$ and $\kappa = 6$. (For interpretation of the references to colour in this figure caption, the reader is referred to the web version of this paper.)

Fig. 3. Effects of noise on clustered ventilation defects; solutions at steady state. (a) Individual simulated trees with varying noise (different noise levels for each row), coloured by normalised radius, with black being zero (closed) and red being 1 (open) as in Fig. 2. (b) Measure of variation (see Appendix A) for each airway in the tree at that noise level (calculated from 100 simulations at each noise level, not just the 5 shown explicitly). The rows are common across panels (a) and (b), each corresponding to the stated noise level. Here $\kappa = 9$, $A = 0.15$, $\hat{q} = 30$. (For interpretation of the references to colour in this figure caption, the reader is referred to the web version of this paper.)
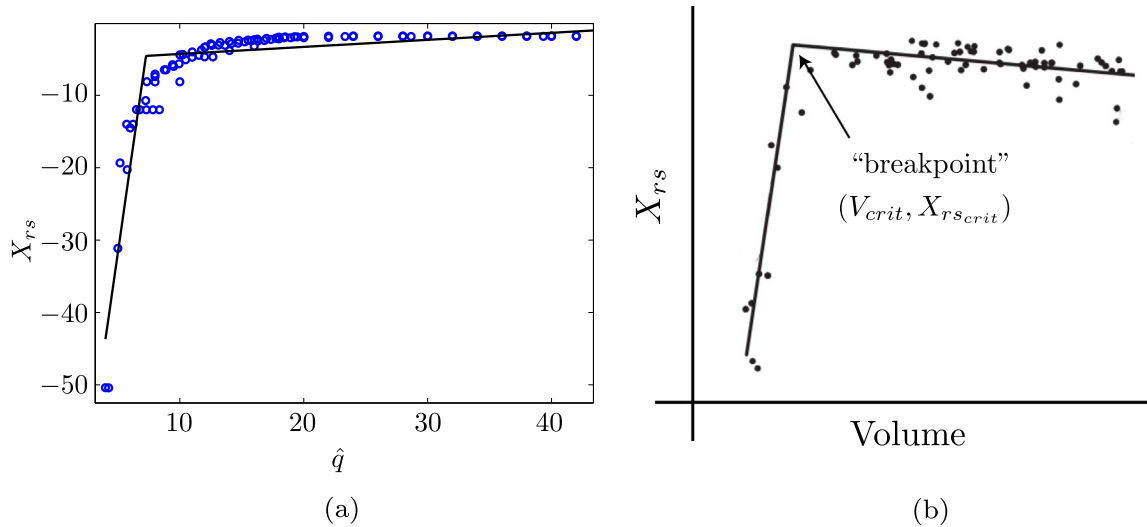
Fig. 4. Bilinear reactance relationships. (a) Stochastic model simulations of reactance X_{rs} versus $\hat{q}$. Blue circles are simulation results, and solid black lines give the bilinear least-squares best fit. Here the parameters are the same as Fig. 2; note that the "breakpoint" here occurs around $\hat{q} \sim 7$, in contrast to the change from heterogeneous to homogeneous ventilation solutions seen in Fig. 2 around $\hat{q} \sim 20$. (b) Breakpoint concept illustration, adapted from Kelly et al. (2013). (For interpretation of the references to colour in this figure caption, the reader is referred to the web version of this paper.)

but vary in their locations across realisations.

We now turn our attention to the bilinear reactance relationship. The concept here is that measured reactance exhibits a characteristic bilinear relationship as volume is varied (Kelly et al., 2012), as schematically illustrated in Fig. 4(b). In the terminology of Kelly et al., the "critical" breakpoint is denoted by the point (V_{crit},
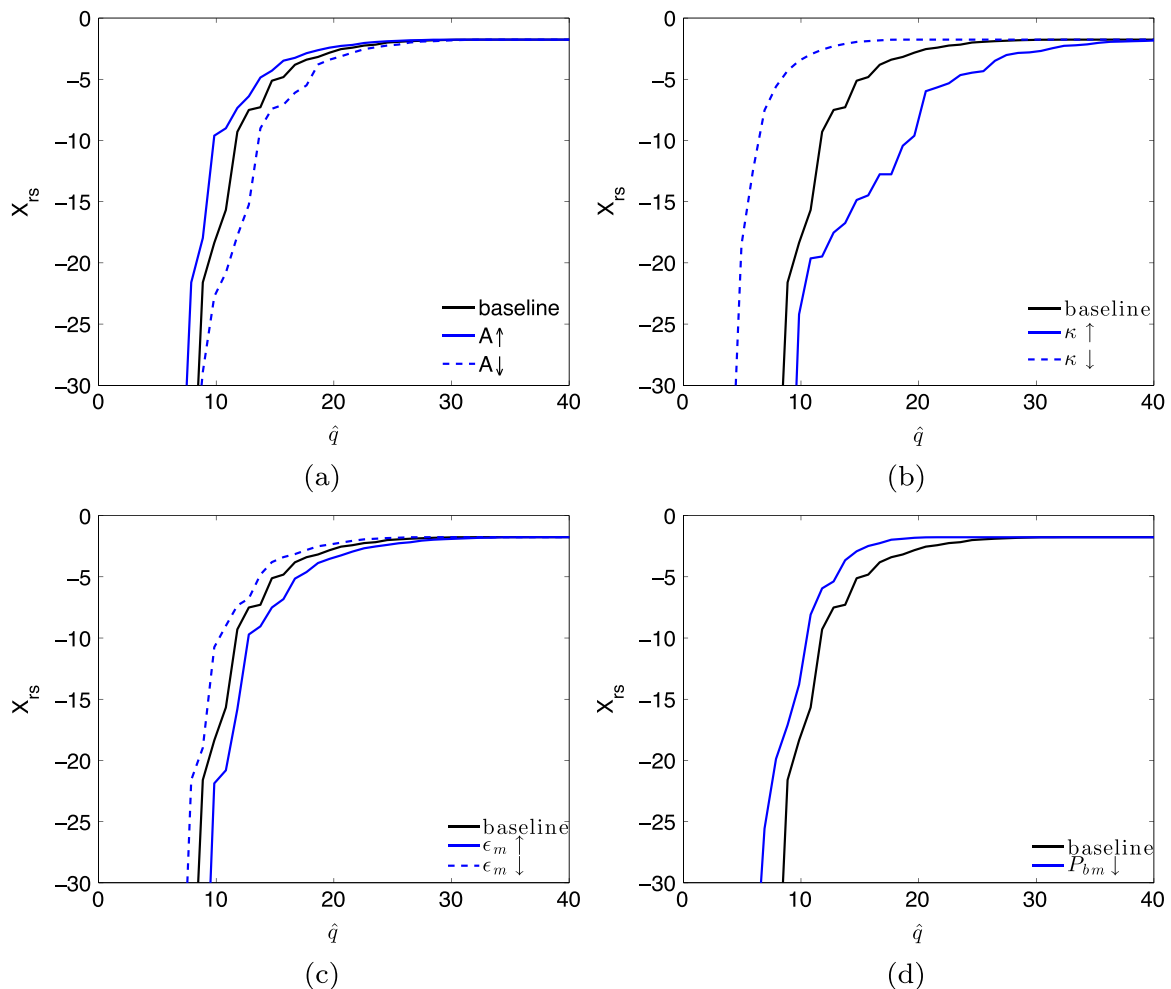
Fig. 5. Sensitivity of reactance relationship to changes in underlying parameters. From top left to lower right, changes in: (a) tethering dependence A, (b) ASM tension κ, (c) airway wall thickness ϵ_m, and (d) basement membrane perimeter.

$X_{\mathrm{rs_{crit}}}$). We can make a similar calculation with the model, with results for typical parameter values given in Fig. 4(a) – here the data are an aggregate of stochastic simulations for multiple trees with depth varying from 9 to 13. Note in comparison that there is no simple relationship between the bifurcation and the breakpoint, with the reactance "breakpoint" occurring around $\hat{q} \sim 7$ (see Fig. 4), while clustered VDefs persist up to $\hat{q} \sim 20$ (Fig. 2).

The parameter values in Figs. 2 and 4 are only representative; of course, altering the underlying structure also influences lung function, and so the parameters associated with the bilinear reactance relationship also change with underlying behaviour. Fig. 5 gives several examples: changing the coupling strength A, changing the ASM tension κ, changing the ASM thickness ϵ_m, and changing the basement membrane perimeter in the small airways (Elliot et al., 2015a). All are plausible alterations which might occur in asthma, and all do indeed alter the reactance output. All changes have some effect on the critical flow value; on the other hand, changes to $X_{\mathrm{rs_{crit}}}$ are less pronounced. Here the simulations are deterministic to reduce computational cost; trees are depth 14.

Another interesting question is the extent to which the explicit inclusion of the conducting airway tree effects the formation of clustered VDefs. Although a full analysis of the model dynamics is beyond the scope of this paper, Fig. 6 contains a numerical exploration of the $A - \kappa$ plane in parameter space. Recall that the parameter A controls the strength of airway–parenchymal coupling, and κ the degree of ASM tension. The four panels are organised as follows: the upper row (panels a and b) contains
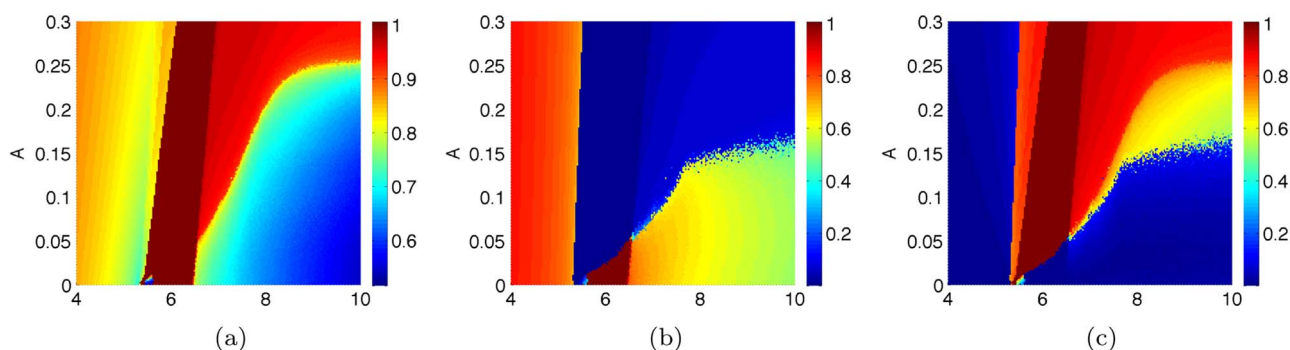
simulation results for trees of depth 9 ($\Delta = 1$), simulated on a relatively fine 400-by-400 grid. The bottom row (panels c and d) is for trees of depth 14 ($\Delta = 1$), but with a coarser 40-by-40 grid due to computational cost. The left column (panels a and c) gives the (normalised) mean cluster size, where clustered solutions exist (white otherwise), and the right column (panels b and d) gives the fraction of open terminal units.

Several key features stand out. First, examining panels (a) and (c), the critical κ value (near $\kappa \sim 5.5$, at which the homogeneous ventilation solution initially loses stability) is relatively insensitive to the coupling strength A. Second, still looking at (a) and (c), for small values of A (and even $A=0$), the region in which clustered VDefs occur is relatively small; this suggests that a larger value of A, where clustered VDefs persist over a larger region of parameter space, is more plausible – given the experimental prevalence of clustered VDefs. And finally, within the "wedge" of clustered solutions, the cluster size dependence is complex, with no simple pattern emerging. Outside of the regions of clustered solutions, we can see by examining panels (b) and (d) that non-clustered solutions are uniformly open, and that within the clustered solution wedge, the open fraction has complex behaviour which has a similar structure to the mean cluster size.

The two sets of simulations for different tree sizes allow an assessment of dependence on this parameter; comparing (a) and (b) with (c) and (d), we see only modest differences with the increase in tree size; while computational cost precludes simulations on sufficiently large trees to mimic a human lung, this
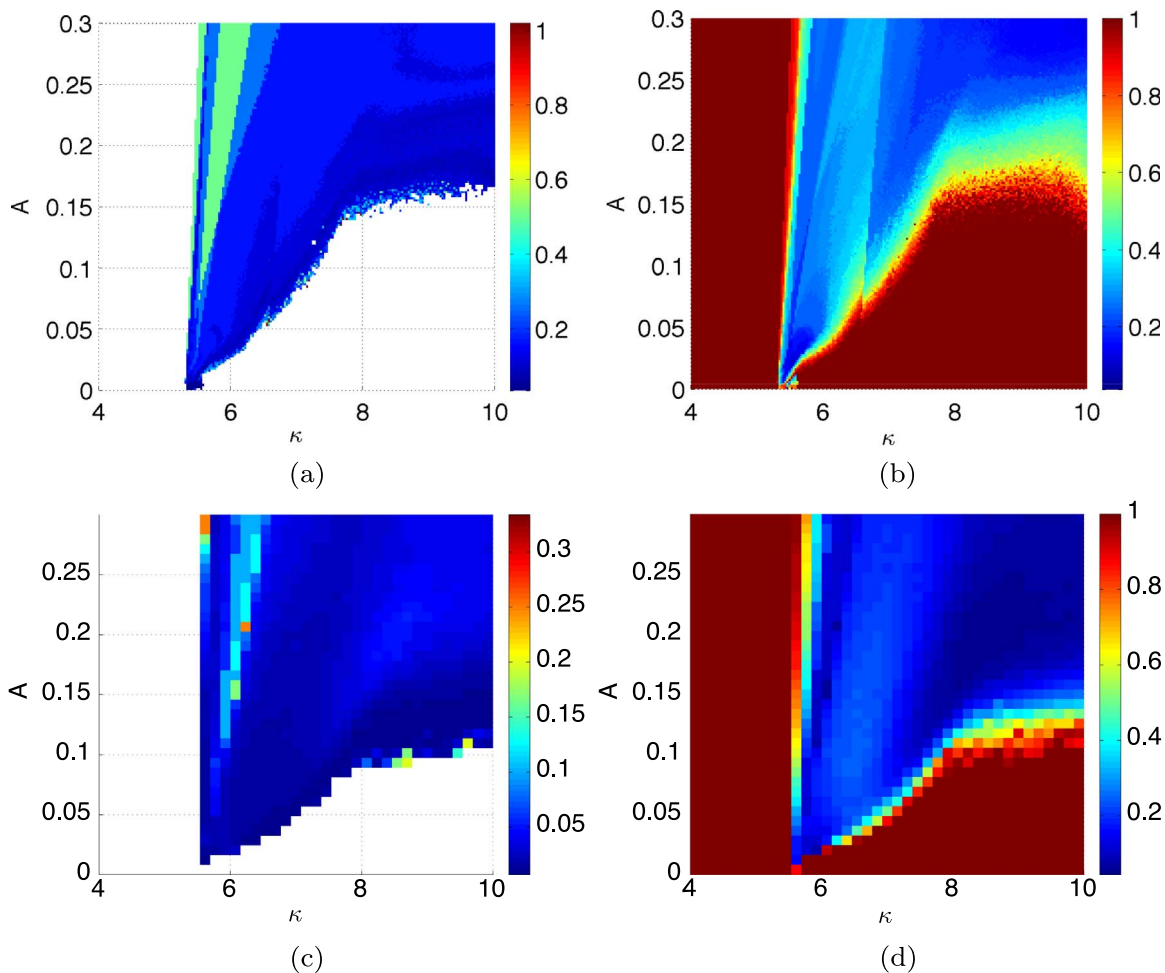
Fig. 6. Numerical exploration of A–κ parameter plane; classification of clustered solutions at steady state. Top row (panels (a) and (b)): simulations with tree depth 9 ($\Delta = 1$), 200 × 200 grid. Bottom row (panels (c) and (d)): simulations with tree depth 14 ($\Delta = 1$), 40 × 40 grid. Left column (panels (a) and (c)): mean cluster size, if solution is clustered (white otherwise; see Appendix A). Right column (panels (b) and (d)): fraction of open airways.

Fig. 7. Simulation results for depth 9, $\Delta = 1$ trees at $\hat{q} = 30$ at steady state across the A–κ plane. (a) Maximum normalised radius of order 1 airways, (b) minimum normalised radius of order 1 airways, (c) range of order 1 airway radii (normalised).

suggests that qualitatively similar behaviour may be expected. Finally, the relatively complex structure suggests that a more detailed analysis of the dynamics, though beyond the scope of this paper, would be worthwhile.

We can also use the same data to more explicitly quantify the solutions at each point in the A–κ plane, in Fig. 7 giving the maximum order 1 radius (panel a), the minimum order 1 radius (b), and the max–min difference (c). This region of the A–κ parameter plane is roughly divided into three regions, a band for small κ in which homogeneous, open states exist; a wedge in which clustered ventilation solutions emerge; and as κ increases further, a region in which homogeneous solutions re-emerge but all airways narrow together.

A further observation from the work of Kelly et al. (2013) is the relationship between distensibility and ASM tone. Kelly et al. define distensibility as the slope of the conductance[10] versus volume curve, in which they evaluate at the key volumes of residual volume (RV), functional residual capacity (FRC), and total lung capacity (TLC). We can also assess the distensibility by computing resistance (see Appendix A) and find a similar relationship: increasing ASM tone (κ) decreases distensibility at all flows; similarly decreasing tone increases distensibility at all flows.

4. Discussion

In this paper we present results from a new model of clustered ventilation defect formation which explicitly incorporates both airway–airway coupling via flow through the conducting tree, and also coupling via tethering dependence (airway–parenchymal interdependence). This construction is based on previous model of Donovan and Kritter (2015) which considered the latter but neglected the former, and also the ideas of Venegas et al. (2005). The initial formulation for this new model resulted in a set of differential-algebraic equations, which presents significant challenges (both computational and theoretical); however, we show that it is possible, for any tree geometry, to eliminate the algebraic constraints and obtain a set of ODEs. This significantly eases both the simulations shown in this paper, and also future analysis. Studying this model, we are able to demonstrate several key findings.

Clustered ventilation defects persist with the inclusion of airway–airway coupling in asymmetric trees, and the locations of these defects are a combination of structural and dynamic factors. In particular, the degree of noise present in the system can create three distinct regimes: a small noise regime wherein ventilation defects occur in only structurally-determined areas; a large noise regime where noise overwhelms other factors and airways become uncoupled; and an intermediate regime wherein switching occurs in the clustering patterns. These findings are in agreement with those of Leary et al. (2014), who also made explicit comparisons with symmetric trees. Though we have only considered structural asymmetries via the branching pattern, it seems plausible that similar mechanisms are at work with other types of structural asymmetries, for example regional or spatially correlated remodelling.

The model exhibits bilinear reactance curves, similar to the bilinear relationship of Kelly et al. (2013). Though the "breakpoint" in this relationship was hypothesised to correspond to recruitment/reopening, here we show that the breakpoint is not coincident with the VDef bifurcation, and that the shape of the reactance curve may instead reflect the highly nonlinear relationship between radius and impedance. While reopening/recruitment is occurring at the breakpoint, it is also happening at other locations, and the breakpoint is not where clustering vanishes. This continues to be true regardless of the interpretation of the underlying data of both this study and Kelly et al. (2012), e.g. whether they are truly bilinear, or rather highly nonlinear saturation. Even in the later case, the bilinear approximation is a useful characterisation.

Changes to bilinear relationship: Because the nature of the bilinear reactance relationship changes with disease (Kelly et al., 2013), it is of interest to see how changes to the underlying model behaviour manifest in terms of changes to the breakpoint analysis. We examined several plausible changes and showed that while each made significant changes in the critical flow point, changes to $X_{rs_{crit}}$ are much less pronounced. This suggests that the mechanism behind changes to $X_{rs_{crit}}$ lies beyond the scope of the model; one plausible candidate in explaining the discrepancy is using flow as a proxy for volume, rather than explicit integration of alveolar volume.

Relationship between distensibility and ASM tone: One key finding of Kelly et al. (2012) was the relationship between distensibility and ASM tone: that is, increasing ASM tone decreases distensibility, and similarly decreasing tone increases distensibility. We find that this relationship indeed persists in the model across the physiological range.

Rich system dynamics in the A–κ plane: Because in vivo values of A and κ are uncertain, it is worthwhile to consider how changes in these parameters alter the behaviour of the system. To this end we conducted an exploration of this parameter space and found several interesting features. First, the critical κ value (at which the initial transition from homogeneous to clustered ventilation occurs) is relatively insensitive to A. Second, while clustered ventilation solutions do exist across the range of A explored, the region of parameter space for which this is true at or near $A=0$ is very small. Given the prevalence of ventilation defects in imaging studies, this suggest a value of A for which VDefs persist in a broader range of κ is more likely.

---

[10] The inverse of the real part of impedance.

As with any modelling study, there are significant assumptions and limitations. Many have been discussed alongside development of the model, but several deserve additional consideration. One, already mentioned with regard to the insensitivity of $X_{rs_{crit}}$, is the use of flow as a proxy for volume in determining the bilinear reactance relationships. This simplification is made to avoid the additional model complexity required to explicitly integrate the flows into acinar volumes. It is also worth noting that we have used an extremely simple treatment of ASM behaviour, even though ASM is known to exhibit a number of rich and interesting phenomena. Similarly, our airway wall model is also relatively simple, employing both quasi-static and thin-walled assumptions (see, by contrast, Brook et al., 2010; Hiorns et al., 2016). Unfortunately at this stage, computational cost precludes a more detailed ASM or wall treatment within a coupling model of any significant scale.[11] Likewise, a more realistic breathing control model is desirable, rather than the simplified extremes of flow- and pressure-control.

Several areas of interest, inspired by the results shown here, are left for future work. For example, the simulation results suggest an interesting bifurcation structure which would merit comprehensive analysis. It would also be interesting to consider the effects of other kinds of structural heterogeneity, for example variation in ASM mass and wall thickness (Elliot et al., 2015b), rather than just tree structure asymmetry.

Acknowledgements

Appendix A. Additional model details

This section gives additional details which are needed to implement the model.

Noise: Simulations with noise convert Eq. (17) into stochastic differential equations (SDEs) with additive zero-mean white noise, which are then simulated numerically using the Euler–Maruyama method (Allen, 2010).

Measure of coherent variation: In Fig. 3, we assess the coherent variation between adjacent airways by computing the covariance matrix across all realisations and taking for each airway the sum of the covariance over its 4 nearest neighbours.

Stopping conditions: Simulations are stopped either when the model reaches steady state (as determined by $\| \dot{\mathbf{r}} \| < 10^{-5}$) or the magnitude of the driving pressure $p_\downarrow$ exceeds 100 cmH$_2$O (deemed to be a generous physiological limit, beyond which strict flow control ceases to be realistic).

Tree generation: As formulated, the model can be used on an arbitrary binary tree. The trees used for computations in this study are the idealised trees of Horsfield et al. (1971), with either $\Delta = 0$ (symmetric trees) or $\Delta = 1$ asymmetry. With these branching rules, trees of arbitrary depth can be generated algorithmically.

Cluster size quantification: Cluster size is defined on order 1 airways by first classifying each airway as open or closed using a threshold of 0.05 mm. Then all groupings of airways in the same state are counted, and the mean of these counts is taken as the mean cluster size.

Impedance: Given solutions to the model as described,

Table A.1
Order-dependent airway wall parameter values; from Politi et al. (2010) and Lambert et al. (1982). The values of P_B are calculated to ensure continuity:
$$P_B = \frac{P_A n_B \left(R_i^2 - r_{i\,max}^2 \right)}{n_A R_i^2}.$$

Order	R_i (mm)	$r_{i\,max}$ (mm)	P_A (Pa)	n_A	n_B	L (mm)
1	0.058	0.296	15.728	1	7	1.700
2	0.065	0.318	17.342	1	7	1.878
3	0.073	0.337	19.475	1	7.185	2.056
4	0.083	0.358	22.747	1	7.778	2.233
5	0.096	0.384	27.140	1	8	2.448
6	0.113	0.414	32.205	1	8	2.685
7	0.132	0.445	39.429	1	8	3.033
8	0.156	0.484	47.104	1	8.148	3.388
9	0.185	0.539	55.704	1	8.741	3.744
10	0.222	0.608	65.407	1	9.333	4.166
11	0.269	0.692	75.968	1	9.926	4.640
12	0.326	0.793	88.028	1	10	5.063
13	0.395	0.913	100.441	1	10	5.511
14	0.475	1.052	113.457	1	10	6.103
15	0.569	1.203	130.989	1	10	6.755
16	0.686	1.374	153.036	1	10	7.466
17	0.840	1.585	174.204	0.952	10	8.274
18	1.026	1.830	195.476	0.893	10	9.125
19	1.244	2.108	218.892	0.833	10	10.133
20	1.537	2.463	251.933	0.774	10	11.218
21	1.908	2.885	297.347	0.715	10	12.403
22	2.315	3.307	349.860	0.656	10	10.433
23	2.791	3.763	415.740	0.6	10	8.022
24	3.410	4.319	646.619	0.6	10	14.777
25	4.261	4.982	1488.249	0.578	10	25.355
26	5.375	5.819	3347.800	0.519	10	42.303
27	6.694	6.995	3928.909	0.5	10	77.096
28	8.157	8.686	3928.909	0.5	10	120.000

respiratory impedance is calculated post hoc using the circuit analogue model of Lutchen and Gillis (1997).

Parameters and units: The model development is given in dimensional terms; following conventions in respiratory physiology, we express pressure in units of cmH$_2$O. Time is in units of s, and radii in mm. (When plotted, airway radii are normalised to their relaxed, fully inflated radius $R_{ref} = R(P_{ref}) = R(25\ \text{cmH}_2\text{O})$.) Thus flow is expressed in mm^3/s, and to account for varying tree size, we scale $\hat{q}$ by the number of terminal units in the tree. As a guide to whole-lung rates, for 30,000 terminal units $\hat{q} = 30$ mm^3/s/(terminal unit) is equivalent to 0.9 l/s. The parameter units are then as follows: $[A] = \text{cmH}_2\text{O s/mm}^3$ and $[\kappa] = \text{cmH}_2\text{O}$. The Poiseuille flow coefficients are $\alpha = 8\mu_d L/\pi$ so $[\alpha] = \text{cmH}_2\text{O·s·mm}$. We take the dynamic viscosity of air at 37C as $\mu_d = 1.95 \times 10^{-7}\text{cmH}_2\text{O·s}$, and airway lengths are taken from Lambert et al. (1982) and given with other order dependent airway parameters in Table A.1. The units of reactance are $[X_{rs}] = \text{cmH}_2\text{O/l/s}$, and the parameter $\rho = 1$ (1/s).

References

Allen, L.J., 2010. An Introduction to Stochastic Processes With Applications to Biology. CRC Press, Boca Raton, FL.

Anafi, R.C., Wilson, T.A., 2001. Airway stability and heterogeneity in the constricted lung. J. Appl. Physiol. 91, 1185–1192.

Brook, B., Peel, S., Hall, I., Politi, A., Sneyd, J., Bai, Y., Sanderson, M., Jensen, O., 2010. A biomechanical model of agonist-initiated contraction in the asthmatic airway. Respir. Physiol. Neurobiol. 170, 44–58.

Donovan, G.M., Kritter, T., 2015. Spatial pattern formation in the lung. J. Math. Biol., 1–31.

Elliot, J.G., Budgeon, C.A., Harji, S., Jones, R.L., James, A.L., Green, F.H., 2015a. The effect of asthma on the perimeter of the airway basement membrane. J. Appl. Physiol., jap-00076

Elliot, J.G., Jones, R.L., Abramson, M.J., Green, F.H., Mauad, T., McKay, K.O., Bai, T.R., James, A.L., 2015b. Distribution of airway smooth muscle remodelling in asthma: relation to airway inflammation. Respirology 20, 66–72.

Golnabi, A.H., Harris, R.S., Venegas, J.G., Winkler, T., 2014. Deep inspiration and the

---

[11] Similarly, computational cost also limits the sizes of simulated trees. The practical upper limit is approximately tree depth 15 for $\Delta = 1$, or about 2000 airways.

emergence of ventilation defects during bronchoconstriction: a computational study. PLoS One 9, e112443.

Hiorns, J.E., Jensen, O.E., Brook, B.S., 2016. Static and dynamic stress heterogeneity in a multiscale model of the asthmatic airway wall. J. Appl. Physiol., jap-00715

Horsfield, K., Dart, G., Olson, D.E., Filley, G.F., Cumming, G., 1971. Models of the human bronchial tree. J. Appl. Physiol., 207–217.

Kaczka, D.W., Brown, R.H., Mitzner, W., 2009. Assessment of heterogeneous airway constriction in dogs: a structure–function analysis. J. Appl. Physiol. 106, 520–530.

Kaczka, D.W., Lutchen, K.R., Hantos, Z., 2011. Emergent behavior of regional heterogeneity in the lung and its effects on respiratory impedance. J. Appl. Physiol. 110, 1473–1481.

Kelly, V.J., Brown, N.J., Sands, S.A., Borg, B.M., King, G.G., Thompson, B.R., 2012. Effect of airway smooth muscle tone on airway distensibility measured by the forced oscillation technique in adults with asthma. J. Appl. Physiol. 112, 1494–1503.

Kelly, V.J., Sands, S.A., Harris, R.S., Venegas, J.G., Brown, N.J., Stuart-Andrews, C.R., King, G.G., Thompson, B.R., 2013. Respiratory system reactance is an independent determinant of asthma control. J. Appl. Physiol. 115, 1360–1369.

Lai-Fook, S., 1979. A continuum mechanics analysis of pulmonary vascular interdependence in isolated dog lobes. J. Appl. Physiol. 46, 419–429.

Lambert, R., Wilson, T., Hyatt, R., Rodarte, J., 1982. A computational model for expiratory flow. J. Appl. Physiol. 52, 44–56.

Layachi, S., Porra, L., Albu, G., Trouillet, N., Suhonen, H., Peták, F., Sevestre, H., Suortti, P., Sovijärvi, A., Habre, W., et al., 2013. Role of cellular effectors in the emergence of ventilation defects during allergic bronchoconstriction. J. Appl. Physiol. 115, 1057–1064.

Leary, D., Winkler, T., Braune, A., Maksym, G.N., 2014. Effects of airway tree asymmetry on the emergence and spatial persistence of ventilation defects. J.

Appl. Physiol. 117, 353–362.

Lutchen, K.R., Gillis, H., 1997. Relationship between heterogeneous changes in airway morphometry and lung resistance and elastance. J. Appl. Physiol. 83, 1192–1201.

Lutchen, K.R., Jensen, A., Atileh, H., Kaczka, D.W., Israel, E., Suki, B., Ingenito, E.P., 2001. Airway constriction pattern is a central component of asthma severity: the role of deep inspirations. Am. J. Respir. Crit. Care Med. 164, 207–215.

Politi, A., Donovan, G., Tawhai, M., Sanderson, M., Lauzon, A., Bates, J., Sneyd, J., 2010. A multiscale, spatially distributed model of asthmatic airway hyper-responsiveness. J. Theor. Biol. 266, 614–624.

Simon, B.A., Kaczka, D.W., Bankier, A.A., Parraga, G., 2012. What can computed tomography and magnetic resonance imaging tell us about ventilation? J. Appl. Physiol. 113, 647–657.

Stewart, P.S., Jensen, O.E., 2015. Patterns of recruitment and injury in a heterogeneous airway network model. J. R. Soc. Interface 12, 20150523.

Tzeng, Y.S., Lutchen, K., Albert, M., 2009. The difference in ventilation heterogeneity between asthmatic and healthy subjects quantified using hyperpolarized 3He MRI. J. Appl. Physiol. 106, 813–822.

Venegas, J.G., Winkler, T., Musch, G., Melo, M.F.V., Layfield, D., Tgavalekos, N., Fischman, A.J., Callahan, R.J., Bellani, G., Harris, R.S., 2005. Self-organized patchiness in asthma as a prelude to catastrophic shifts. Nature 434, 777–782.

Winkler, T., Venegas, J.G., 2007. Complex airway behavior and paradoxical responses to bronchoprovocation. J. Appl. Physiol. 103, 655–663.

Winkler, T., Venegas, J.G., Harris, R.S., 2015. Mathematical modeling of ventilation defects in asthma. Drug Discov. Today: Dis. Model. 15, 3–8.

Wongviriyawong, C., Winkler, T., Harris, R.S., Venegas, J.G., 2010. Dynamics of tidal volume and ventilation heterogeneity under pressure-controlled ventilation during bronchoconstriction: a simulation study. J. Appl. Physiol. 109, 1211–1218.